Transmission of Depth Data by Pulse Position Modulation for Underwater Acoustic Positioning Systems

Atsushi Wada, Shingo Yoshizawa
Kitami Institute of Technology, Kitami, Hokkaido 0908507, Japan

Received: September 23, 2021. Revised: March 14, 2022. Accepted: April 18, 2022. Published: May 30, 2022.

Abstract—This paper presents a three dimensional localization method for underwater acoustic positioning systems. In typical ultra-short baseline (USBL) acoustic positioning systems, the three dimensional position is localized by using multiple time difference of arrivals (TDOAs). Since the TDOA accuracy is less than the other sensor data, we focus on a localization method with the minimum number of TDOA. We propose a method of transmitting depth data by pulse position modulation (PPM), where the target position is localized by a single TDOA, a distance, and a depth. The proposed method shows a higher positional accuracy than the conventional method with two TDOAs. The effectiveness of the proposed method has been demonstrated in the evaluation of simulation and experiment.

Keywords— underwater acoustic positioning, time difference of arrival, pulse position modulation, multipath interference

I. INTRODUCTION

AN underwater acoustic positioning system (UAPS) is used for tracking and navigating underwater vehicles such as remotely operated vehicles (ROVs) and autonomous underwater vehicles (AUVs) [1]. In addition, the UAPS is essential for the sensor nodes to be aware of their positions in underwater acoustic sensor networks [2].

The operation methods of UAPS are generally categorized into three types called long baseline (LBL), short baseline (SBL), and ultra-short baseline (USBL). USBL uses a small array of receiver hydrophones and estimates arrival of angles (AOAs) of a sound source and a distance between a sound source and a receiver element.

In the AOA estimation, time difference of arrival (TDOA) measurement, which makes a cross correlation function between two received signals and measures a time difference, is widely used [3]-[8]. In the TDOA measurement, matched filter (MF) [3]-[4], generalized cross-correlation with phase transform (GCC-PHAT) [5], and zero-crossing [6] algorithms have been studied in the related works. In our previous work, we discussed impulse response based GCC-PHAT (IR-GCC-PHAT) as a countermeasure to multipath interference [7]-[8]. IR-GCC-PHAT shows a higher positional accuracy than the other algorithms in a shallow water environment.

In typical USBL systems, the three dimensional position is localized by using multiple TDOAs [9]-[10]. For example, the relative position of a sound source is computed from a distance between a sound source and a receiver and two TDOAs [11]. However, the accuracy of TDOA is less than the other sensor data, such as a distance and a water depth. We focus on a localization method with the minimum number of TDOA in order to improve the position accuracy.

We study a different approach that the target position is localized by a single TDOA, a distance, and a depth. The depth information is available through a depth sensor. In [12], a sensor suite consisted of an underwater camera, an inertial measurement unit, a sonar, and a depth (pressure) sensor for underwater reconstruction. The key issue is how to send depth data through underwater wireless communication. The combination of an acoustic positioning unit and an acoustic modem has been demonstrated in [13]. However, data communication processing of spread spectrum (SS) modulation is quite burdensome compared with acoustic positioning.

We propose a method of transmitting depth data by pulse position modulation (PPM). The use of PPM in underwater acoustic communication has been discussed in [14]. PPM modulates information to signal position and demodulates it by detecting a peak position in a correlation function. Since the transmit signal pattern is fixed, PPM can be realized by adjusting a transmit signal timing. The PPM signal structure and the encoding/decoding of depth data are also discussed.

This paper is organized as follows. Section II explains the three dimensional localization methods. Section III presents the transmission of depth data based on PPM. Section IV reports the simulation and experimental results of acoustic positioning. Section V describes the discussion about the evaluation results. Section IV summarizes our work.

II. THREE DIMENSIONAL LOCALIZATION

A. Estimation of AOA

When coordinates of a r-th receiver element are represented by $\boldsymbol{p}_r = [x_r, y_r, z_r]$ and those of a transmitter (a sound source) are given by $\boldsymbol{q}_\mathrm{t} = [x_\mathrm{t}, y_\mathrm{t}, z_\mathrm{t}]$, a distance between a r-th receiver and a transmitter becomes $R_r = \|\boldsymbol{p}_r - \boldsymbol{q}_\mathrm{t}\|$. The TDOA between the first and r-th receiver elements can be modeled as

$$\tau_{r1} = (R_r - R_1)/c, \tag{1}$$

where c denotes a sound velocity. The TDOA can be measured by taking a cross correlation for two received signals, where various types of TDOA measurement algorithms (MF, GCC-PHAT, zero-crossing, and IR-GCC-PHAT [3]-[8]) can be applied. After the TDOA is measured, the AOA is computed as

$$\theta_{r1} = \arccos(c\tau_{r1}/d), \tag{2}$$

where d denotes an array space between the receiver elements.

B. Measurement of Distance

We assume that a transmitter and a receiver have the same clock time. In [15], the time synchronization was achieved by integrating a chip-scale atomic clock (CSAC) into an acoustic modem. When the transmitter sends a signal to the first receiver element, the receiver observes it at the arrival time t_1. The distance between the first receiver element and the transmitter becomes $R_1 = ct_1$.

The TDOA can also be measured by comparing the arrival times between the receiver elements, e.g., $\tau_{r1} = t_1 - t_r$. This way is equivalent to MF algorithm that the time difference is measured by detecting every peak position in cross correlation functions. If three types of arrival times (e.g., t_1, t_2, and t_3) are available, they can be converted into two TDOAs ($\tau_{21}$and τ_{31}) and one distance (R_1).

C. Localization with Multiple TDOAs

The localization with multiple TDOAs is illustrated in Fig. 1. We treat the case of two TDOAs (τ_{21} and τ_{31}) using three receiver elements ($\boldsymbol{p}_1$, $\boldsymbol{p}_2$, and $\boldsymbol{p}_3$) for simplicity. The AOAs of θ_{21} and θ_{31} correspond to azimuth and elevation angles. The distance between the transmitter and the first receiver element is represented by R_1. When the first receiver element is located at the point of origin, the coordinates of the transmitter can be localized as

$$\begin{aligned} x_\mathrm{t} &= R_1 \cos\theta_{21} \\ y_\mathrm{t} &= R_1 \sqrt{1 - \cos^2\theta_{21} - \cos^2\theta_{31}} \\ z_\mathrm{t} &= R_1 \cos\theta_{31}. \end{aligned} \tag{3}$$

The AOAs are sensitive to estimated errors because a time difference is converted to an angle as shown in (2). When the value of $c\tau_{r1}/d$ is near 1, a slight deviation induces a significant angle difference.

D. Localization with a Single TDOA

The localization with a single TDOA is shown in Fig. 2. With the depth D_t, the coordinates of the transmitter are localized as

$$\begin{aligned} x_\mathrm{t} &= R_1 \cos\theta_{21} \\ y_\mathrm{t} &= R_1 \sqrt{1 - \cos^2\theta_{21} - (D_\mathrm{t}/R_1)^2} \end{aligned}$$

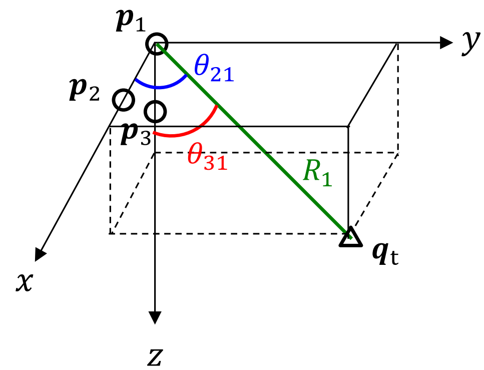

Figure 1. Localization with multiple TDOAs.

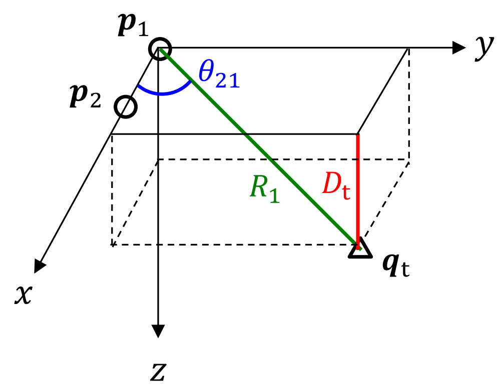

Figure 2. Localization with a single TDOA.

$$z_\mathrm{t} = D_\mathrm{t}. \tag{4}$$

The depth can be measured by a depth sensor. The accuracy of a depth sensor is given by several centimeters (See Section III.A). The advantage of measuring a depth is that it is less sensitive to disturbances such as reflection of sound waves.

III. Transmission of Depth Data

A. Depth Sensor

A depth sensor converts an underwater pressure value into a position from water surface. We used the Blue Robotics Bar30 depth/pressure sensor, which can measure up to 30 bar (300 m depth). Figure 3 shows the depth sensor that we made. The Bar30 sensor, an Arduino Nano computer, and a USB repeater are enclosed in a water-resistant container. We evaluated three depth sensors in a swimming pool, where their depth values were measured by changing a position along the z-axis in the water.

DOI: 10.46300/9106.2022.16.122 Volume 16, 2022

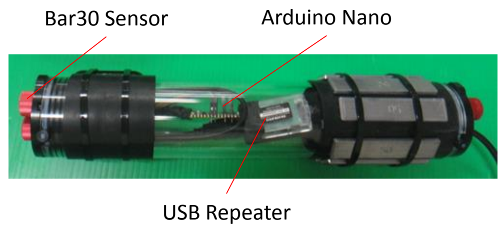

Figure 3. Depth sensor unit.

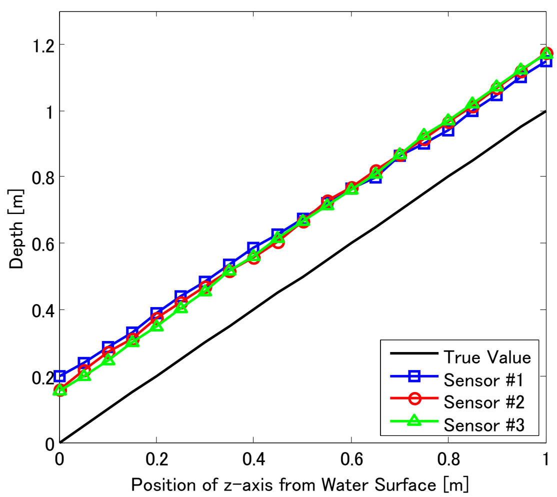

(a) without calibration

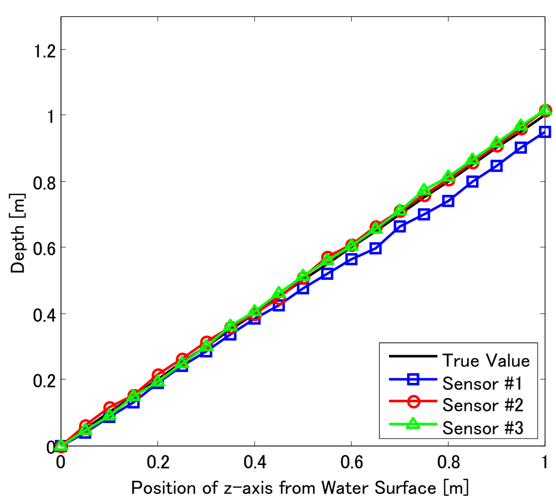

(b) with calibration

Figure 4. Measurement results of depth sensor units.

The measurement results are shown in Fig. 4. Figure 4(a) shows the results without calibration. Although the three sensors have an offset of approximately 0.2 meters, the measured depths are proportional to the z-axis position. Figure 4(b) shows the results with calibration that their offset values are compensated. The average errors are 3 cm, 9 mm, and 9 mm for each of the three sensors. As long as the depth sensor is properly calibrated, the depth can be measured in the order of several centimeters.

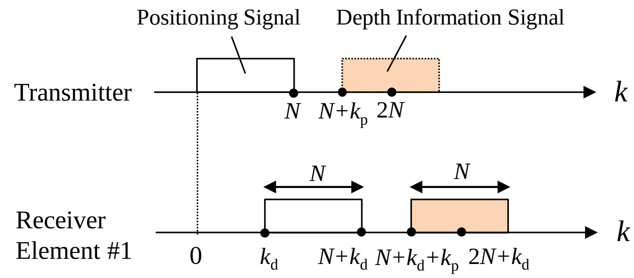

Fig. 5 Signal structure and timing chart of PPM.

B. Depth Data Transmission by PPM

If the depth sensor is connected to the receiver through a wired communication cable, the depth data are easily available. Otherwise, we should consider sending the depth data via underwater wireless communication. The combination of an acoustic positioning unit and an acoustic modem was demonstrated in [13]. In [13], binary PSK and direct sequence spread spectrum (DSSS) is adopted in primary and secondary modulations. The modulation/de-modulation processing is quite heavy in relation to the acoustic positioning because it is necessary to implement specialized functions of the communication into the transmitter.

We adopt a simple data transmission method by PPM [14]. PPM modulates information to a signal position and demodulates it by detecting peak position in a correlation function. Since the transmit signal pattern is fixed, PPM can be achieved by adjusting a signal transmit timing.

The signal structure and the timing chart are shown in Fig. 5. The transmitter and the receiver are assumed to have the same clock time. For the discrete time k, the lengths of the positioning signal and the depth information signal are given by N samples. The transmitter starts sending the positioning signal at the timing of $k = 0$. The receiver (at the receiver first element) accepts the signal head at $k = k_\mathrm{d}$. It corresponds to the propagation time of $t_1 = k_\mathrm{d}/F_\mathrm{s}$, where F_s is a sampling frequency. The positioning signal is used for the measurement of the distance and the time difference between the receiver elements.

The start time of the depth information signal varies between N and $2N$ according to a depth value. Given the depth range as $0 \leq D_\mathrm{t} \leq D_\mathrm{max}$, the transmitter starts sending the positioning signal at the timing of $k = N + k_\mathrm{p}$, where the time offset k_p is represented as

$$k_\mathrm{p} = \lfloor N D_\mathrm{t}/D_\mathrm{max} \rfloor. \tag{5}$$

The resolution of the depth is given by $\Delta D = D_\mathrm{max}/N$. It becomes 0.61 mm in the case of D_max=10 m and N=16384. This resolution is enough as long as acoustic positioning is performed in a shallow water environment.

The receiver accepts the signal head at the time of $N + k_\mathrm{d} + k_\mathrm{p}$. Since k_d is obtained from the distance measurement, k_p is estimated by detecting the depth information signal based on a cross correlation function. The depth D_t is calculated by

$$D_\mathrm{t} = k_\mathrm{p} D_\mathrm{max}/N. \tag{6}$$

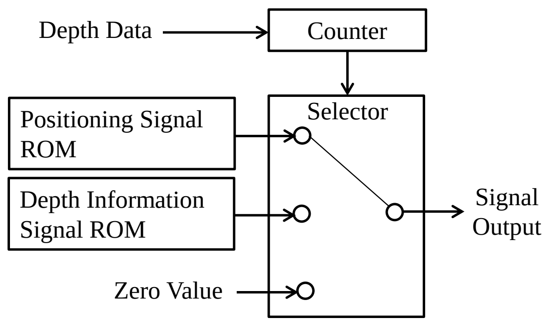

Figure 6. Block diagram of transmitter.

The transmission of the depth data by PPM can easily be implemented into the transmitter. A block diagram of the transmitter is shown in Fig. 6. Since the positioning signal pattern and the depth information signal pattern are fixed, their signal data can be stored in read only memory (ROM). The signal output is controlled by the selector where the start time of sending the depth information signal depends on the depth value.

IV. Simulation and Experiment

A. Simulation Condition

The pseudo noise signals are generated from a sequence of PN codes for the use of the positioning signal and the depth information signal. Their signal length is 16384 samples and corresponds to 65.5 ms for the sampling frequency of 250 kHz. The transmitted signal frequency band is from 12 kHz to 32 kHz. The array space of the receiver elements is 0.3 m. The acoustic field size is 12 × 30 × 6.87 m (length, width, and height). The reflectance ratios are 1 for the water surface and 0.7 for the water bottom and other surrounding walls. The sound velocity is 1480 m/s.

The locations of the transmitter and the first receiver element are shown in Fig. 7. The location of the transmitter is changed every 2.5 m on the x-axis (10 to 25 m) and 2 m on the y-axis (2 to 6 m). The depth of the transmitter is set to 1 m, which is 5.87 m in the z-axis. The coordinates of the first, second, and third receiver elements ($\boldsymbol{p}_1$, $\boldsymbol{p}_2$, and $\boldsymbol{p}_3$) are [6, 5, 5.87], [5.7, 5, 5.87], and [6, 5, 5.57], respectively.

In the signal modeling, we use a sound wave propagation simulator [16]. The impulse response is obtained by determining the size of acoustic field, the reflectance ratios, and the positions of transmitter and receiver elements. The uncorrelated noise is added into a transmit signal. The amplitude of additive white Gaussian noise (AWGN) is adjusted by a signal-to-noise ratio (SNR) setting value. The SNR is set to 30 dB in this simulation.

We evaluate the position errors where these errors are evaluated by the Euclidean distance between true and measured positions. The conventional method is given by the localization with two TDOAs, where the position is calculated in (3). The localization of the proposed method is done by a single TDOA and the depth data transmission, where the position is calculated in (4). Since the accuracy of a depth sensor is much

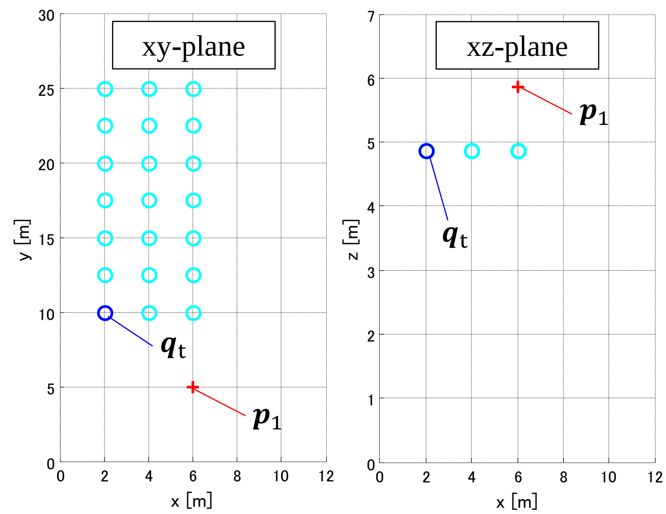

Figure 7. Locations of transmitter and first receiver element.

higher than the TDOA measurement, we assume that the depth is ideally measured. In the TDOA measurement algorithm, we apply shortened impulse response based GCC-PHAT (SIR-GCC-PHAT) [8] for both methods. SIR-GCC-PHAT is the most robust against of sound wave reflections.

B. Simulation Results

The simulation results of the conventional and the proposed methods are shown in Fig. 8 and Fig. 9. The measured positions are plotted on the xy- and xz-planes. When viewed from the xy-plane, there is not much difference in positioning accuracy between the conventional and the proposed methods. As for the xz-plane, the proposed method provides a stable position accuracy compared with the conventional method. It comes from the difference that the position on the z-axis is determined by the elevation angle or the depth data.

The average errors of the conventional and the proposed methods are 0.84 m and 0.17 m. The average errors for the measurement types are reported in Table 1. The distance is measured in the order of centimeters. The azimuth angle is more precise than the elevation angle. The depth data transmission enables an accuracy of the order of centimeters. Since the measurement errors are mostly due to the estimation of the azimuth and elevation angles, the proposed method that takes the minimum number of TDOA is effective in three dimensional localization.

C. Experimental Condition

We conducted the experiment of underwater positioning in the large water tank. Figure 10 shows the experimental scenery. The acoustic field size and the positions of the transmitter and receiver elements are the same as in the simulation. The transmitted signal was made by the software and transmitted via a digital-to-analog converter (DAC), an amplifier, and a transducer. The received signals were recorded from an analog-to-digital converter (ADC) output. The SNR is given by the ratio of the received power when the transmitted signal was

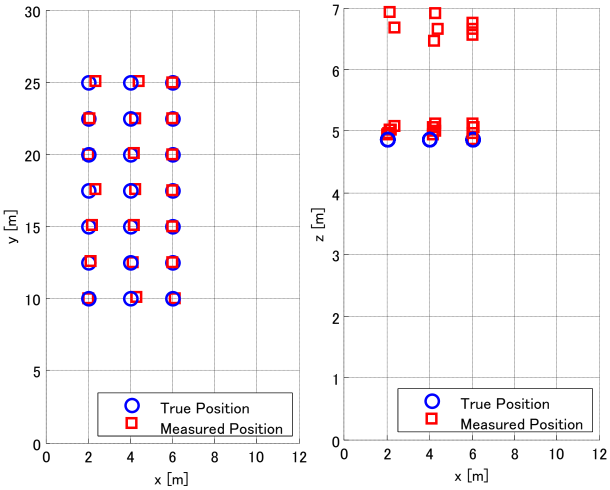

Figure 8. Simulation results for the conventional method.

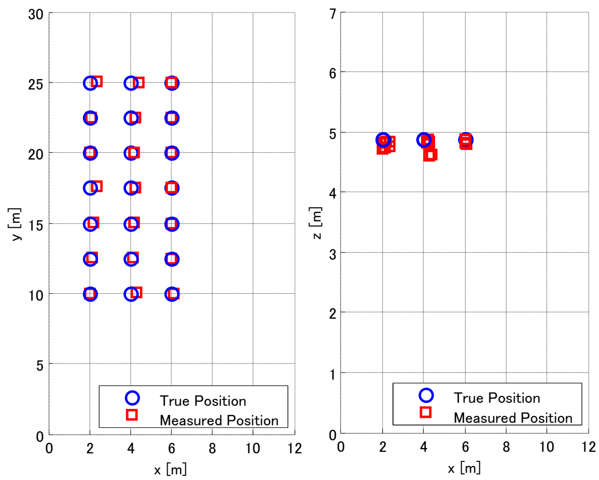

Figure 9. Simulation results for the proposed method.

Table 1. Simulation results for measurement types.

Measured type	Average error
Distance	0.0098 m
Azimuth angle	0.81 deg (0.15 m on xy-plane)
Elevation angle	2.85 deg (0.79 m on z axis)
Depth data transmission	0.067 m

being transmitted and the noise power when the transmission was stopped. The average SNR was 33 dB.

D. Experimental Results

The experimental results of the conventional and proposed methods are shown in Fig. 11 and Fig. 12. There is not much difference in positional accuracy between the conventional and the proposed methods when viewed from the xy-plane. The conventional method has large errors in the position on the z-axis as well as the simulation results. The average errors of the conventional and the proposed methods are 0.95 m and 0.19 m.

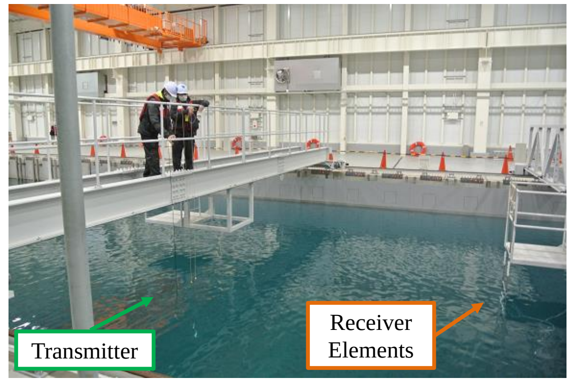

Figure 10. Experimental scenery

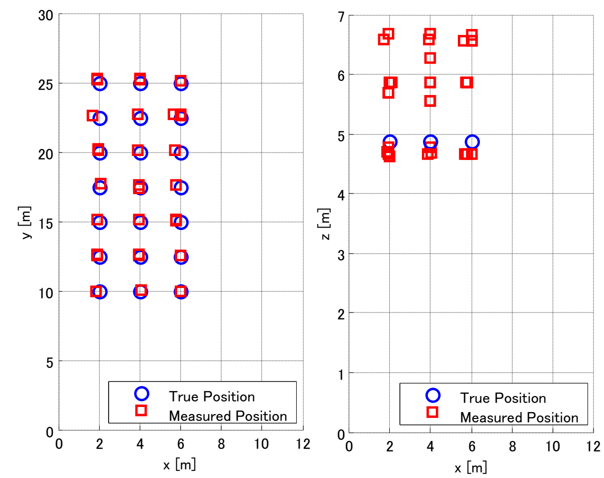

Figure 11. Experimental results for the conventional method.

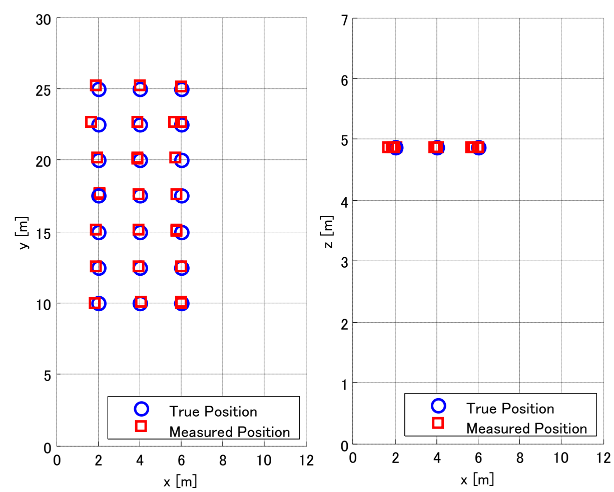

Figure 12. Experimental results for the proposed method.

The average errors for the measurement types are reported in Table 2. The accuracy of distance measurement was degraded with respect to the simulation. The trends of azimuth angle, elevation angle, and depth data transmission are similar those in the simulation. The proposed method has shown a higher

Table 2. Experimental results for measurement types.

Measured types	Average error
Distance	0.13 m
Azimuth angle	0.38 deg (0.19 m on xy-plane)
Elevation angle	3.93 deg (0.91 m on z axis)
Depth data transmission	0.026 m

positional accuracy than the conventional method as well in the experiment.

V. Discussion

A. Influence of Sound Wave Reflections

The influence of positioning accuracy for sound wave reflections can be analyzed from the impulse response that expresses acoustic reflection paths between a sound source and a receiver. A received signal $y_r(k)$ is modeled by using a transmitted signal $x(k)$ and an impulse response $h_r(k)$ for an r-th receiver element as

$$y_r(k) = h_r(k) * x(k) + n_r(k) \tag{7}$$

where k indicates a discrete time index and $*$ shows a convolution operation. $n_r(k)$ is noise component uncorrelated with the transmitted signal.

The calculation of a cross correlation function between a transmit signal and a reference signal is adopted in the distance measurement, the TDOA measurement (MF and IR-GCC-PHAT algorithms), and the detection of depth information signal. The computation of cross correlation is equivalent to estimating the impulse response (see Section II.C in [7]).

An example of the impulse response is illustrated in Fig. 13. The impulse response is generated by using a sound wave propagation simulator. In this example, the coordinates of transmitter and the first receiver element are set to [4, 20, 4.87] and [6, 5, 5.87]. There are two large correlation peaks labeled as A_0 and A_1. The peak A_0 is derived from the direct wave that a sound wave reaches directly from a transmitter to a receiver. The peak A_1 is caused by the reflected wave that a sound wave reflects on water surface and reaches a receiver. Their normalized amplitudes are 1 and 0.983. If the impulse response is ideally estimated, this peak difference can be detected. It is difficult to detect it due to the uncertainty related to noise components in (7) and the limitation of time resolution.

Let us consider the influence of mistaking the peak A_1 for the peak A_0. The difference of their arrival times is $\Delta t = 0.18$ ms, which corresponds to $\Delta k = 45$ samples. In the distance measurement, the distance error is $c\Delta t$=0.26 m. In the depth data transmission, the depth error is 0.0275 m computed from (6) substituting $k'_{\mathrm{p}} = k_{\mathrm{p}} + \Delta k$. Concerning the TDOA measurement, we assume that the direct wave is detected at the first receiver element and the reflected wave is detected at the second receiver element. The angle error can be calculated from (2) substituting $\tau'_{r1} = \tau_{r1} + \Delta t$. The angle error becomes

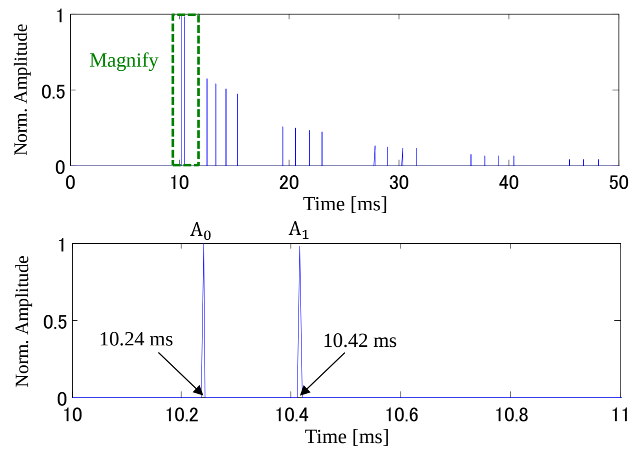

Figure 13. Impulse response and peak positions.

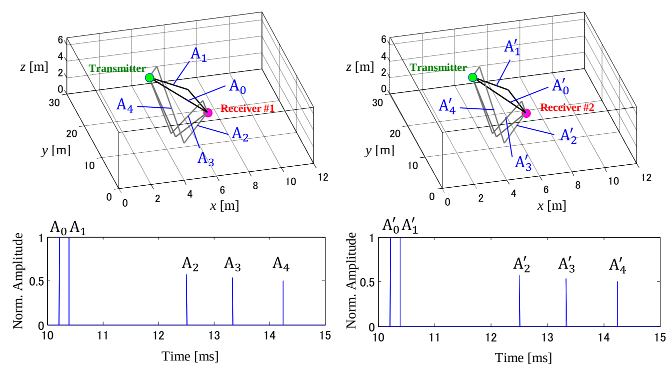

(a) First receiver element (b) Second receiver element

Figure 14. Acoustic paths and impulse responses for first and second receiver elements.

1.96 degree in the worst case. The TDOA measurement is most sensitive to the influence of sound wave reflections.

B. Azimuth and Elevation Angles

We discuss the measurement errors for azimuth and elevation angles. Figure 14 shows acoustic paths and impulse responses from the transmitter to the first and second receiver elements. The second receiver element is located at [5.7, 5, 5.87]. The locations of the transmitter and the first receiver elements are identical in Section V.A. There are many acoustic paths that a sound wave reflects on water surface, bottom, and side walls. This figure displays only acoustic paths that reflected on water surface and bottom.

Due to the sound wave reflections, the pseudo peaks of A_1, A_2, A_3, and A_4 (A'_1, A'_2, A'_3, and A'_4) are observed on the impulse responses. As explained in Section V.A, the confusion between the peak A_0 and the peak A_1 (A'_0 and A'_1) induces large errors in the AOA estimation. When we look at the acoustic paths on the xy-plane in Fig. 14, the arrival angles in the horizontal direction are identical independently of the direct and the reflected waves. It indicates that the time difference between A_0 and A'_0 is the same as that between A_1 and A'_1. IR-GCC-PHAT emphasizes only this time difference by taking the cross correlation function for the two impulse responses and can reduce the measurement errors compared with MF (See

Section V.B in [8] for the details). The azimuth angles are correctly estimated by using IR-GCC-PHAT algorithm, as shown in the simulation and experimental results on the xy-plane in Fig. 9 and Fig. 11.

The relationship between the elevation angles and the sound wave reflection can also be investigated by observing the acoustic paths. When we look at the acoustic paths of A_0, A_1, A_2, A_3, and A_4, their arrival angles in the vertical direction are inconsistent. It is difficult to improve the accuracy of TDOA measurement from the vertical receiver array ($\boldsymbol{p}_1$ and $\boldsymbol{p}_3$ in Fig. 1) even if we apply IR-GCC-PHAT. This is the reason that azimuth angle estimation is adopted in the proposed method.

C. Localization with Two Azimuth Angles

The conventional method could be implemented by using two azimuth angles. The localization with two azimuth angles is illustrated in Fig. 15. The coordinates of the transmitter are expressed as

$$\begin{aligned} x_t &= R_1 \cos\theta_{21} \\ y_t &= R_1 \cos\theta_{31} \\ z_t &= R_1 \sqrt{1-\cos^2\theta_{21}-\cos^2\theta_{31}}. \end{aligned} \qquad (8)$$

The azimuth angles are expected to be accurately estimated by IR-GCC-PHAT. The simulation results are shown in Fig. 16. Unfortunately, the use of two azimuth angles cannot improve positioning accuracy. The error average is 1.55 m, which is worse than in Fig. 8. This is due to the sensitivity of $\sqrt{1-\cos^2\theta_{21}-\cos^2\theta_{31}}$ appeared in (3) and (8). When the elevation angle is estimated in a shallow water environment, $\cos\theta_{31}$ are nearly zero in most cases. The vertical position is mostly determined by only $\cos\theta_{21}$ (however, the accuracy of AOA is worse than in the depth data transmission). On the use of two azimuth angles, $\cos\theta_{21}$ and $\cos\theta_{31}$ depend on the transmitter location and their range is wide. With respect to acoustic positioning in a shallow environment, the estimation of azimuth and elevation angles is desirable rather than the estimation of only azimuth angles.

VI. Conclusion

This paper has presented a method of depth data transmission for underwater acoustic positioning systems. We explained the methods of a single and multiple TDOAs in the three dimensional localization. Since the use of a single TDOA requests wireless transmission of depth data, we have proposed the transmission of depth data based on PPM. The proposed method achieves a higher positional accuracy than the conventional method in the evaluation of simulation and experiment. Furthermore, the influence of positioning accuracy for sound wave reflections has been analyzed from the acoustic propagation simulation.

Our future work will focus on the implementation of an acoustic positioning system for underwater vehicle navigation. The design and experimental validation of a USBL positioning system will be discussed.

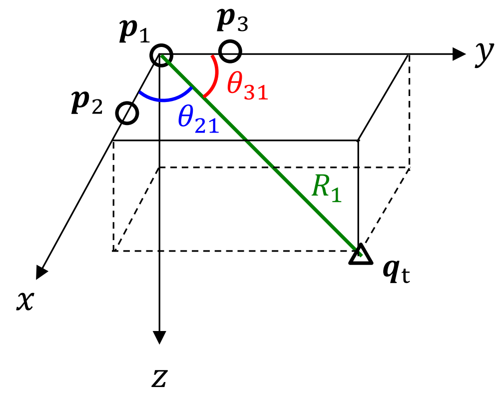

Figure 15. Localization with two azimuth angles.

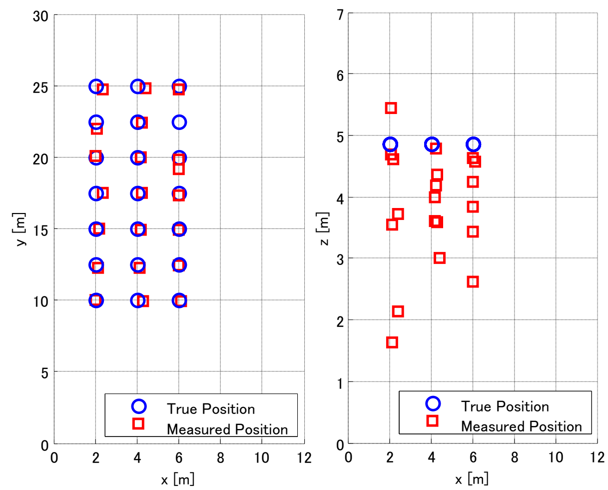

Figure 16. Simulation results for using two azimuth angles.

Acknowledgment

This work was supported by JSPS KAKENHI Grant Number 20K04477.

References

[1] L. Paull, S. Saeedi, M. Seto, and H. Li, "AUV navigation and localization: a review," IEEE Journal of Oceanic Engineering, vol. 39, no. 1, pp. 131-149, Jan. 2014.

[2] M. T. Isik and O. B. Akan, "A three dimensional localization algorithm for underwater acoustic sensor networks," IEEE Transactions on Wireless Communications, vol. 8, no. 9, pp. 4457-4463, Sep. 2009.

[3] J. Reis, M. Morgado, P. Batista, P. Oliveira, and C. Silvestre, "Design and experimental validation of a USBL underwater acoustic positioning system," MDPI Sensors, vol. 16, issue 9, 23 pages, June 2016.

[4] B. Kouzoundjian, F. Beaubois, S. Reboul, and J. B. Choquel, and J. Noyer, "A TDOA underwater localization approach for shallow water environment," MTS/IEEE OCEANS 2017 - Aberdeen, pp. 1-4, June 2017.

[5] J. Choi, J. Park, Y. Lee, J. Jung, and H. Choi, "Robust directional angle estimation of underwater acoustic

sources using a marine vehicle," MDPI Sensors, vol. 18, issue 9, pp. 1-14, Sep. 2018.

[6] J. F. Valente and J. C. Alves, "Real-time TDOA measurements of an underwater acoustic source," MTS/IEEE OCEANS 2016 - Monterey, pp. 1-7, Sep. 2016.

[7] S. Yoshizawa, "Underwater acoustic localization based on IR-GCC-PHAT in reverberant environments," International Journal of Circuits, Systems and Signal Processing, vol. 15, pp.164-171, Mar. 2021.

[8] S. Yoshizawa, "Impulse response shortening in TDOA algorithm for underwater acoustic localization," International Journal of Circuits, Systems and Signal Processing, vol. 15, pp.1624-1631, Nov. 2021.

[9] T. Zhang, J. Wang, L. Zhang, and L. Guo, "A student's T-based measurement uncertainty filter for SINS/USBL tightly integration navigation system," IEEE Transactions on Vehicular Technology, vol. 70, no. 9, pp.8627-8638, Sep. 2021.

[10] M. Morgado, P. Oliveira, and C. Silvestre, "Experimental evaluation of a USBL underwater positioning system," IEEE ELMAR-2010, pp. 485-488, Sep. 2010.

[11] L. Zhang, T. Zhang, H. -S. Shin and X. Xu, "Efficient underwater acoustical localization method based on time difference and bearing measurements," IEEE Transactions on Instrumentation and Measurement, vol. 70, pp.1-16, Dec. 2020.

[12] S. Rahman, N. Karapetyan, A. Q. Li, and I. Rekleitis, "A modular sensor suite for underwater reconstruction," MTS/IEEE OCEANS 2018 - Charleston, pp.1-6, Oct. 2018.

[13] Y. Watanabe, Y. Ota, S. Ishibashi, T. Shimura, M. Sugesawa, and K. Tanaka, "An ocean experiment of inverse SSBL acoustic positioning using underwater vehicle OTOHIME," MTS/IEEE OCEANS 2016 - Monterey 2016, pp. 1-5, Dec. 2016.

[14] T. Zheng, F. Zhou, and W. Zheng, "Pulse position modulation spread spectrum underwater acoustic communication system using N-H sequence," IEEE International Conference on Signal Processing, Communications and Computing (ICSPCC), pp. 1-4, Nov. 2016.

[15] K. G. Kebkal, O. G. Kebkal, I. Glushko, V. Kebkal et.al, "Underwater acoustic modems with integrated atomic clocks for one-way travel-time underwater vehicle positioning," 4th Underwater Acoustics Conference and Exhibition, pp. 315-323, Sep. 2017.

[16] D. R. Campbell, K. J. Palomaki, and G. J. Brown, "Roomsim, a MATLAB simulation of shoebox room acoustics for use in teaching and research," Computing and Information Systems Journal, vol. 9, issue 3, pp. 1-4, Oct. 2005.